

Problem-Fluent Models for Complex Decision-Making in Autonomous Materials Research

Soojung Baek¹ and Kristofer G. Reyes*¹

¹Department of Materials Design and Innovation, University at Buffalo

Abstract

We review our recent work in the area of autonomous materials research, highlighting the coupling of machine learning methods and models and more problem-aware modeling. We review the general Bayesian framework for closed-loop design employed by many autonomous materials platforms. We then provide examples of our work on such platforms. We finally review our approaches to extend current statistical and ML models to better reflect problem specific structure including the use of physics-based models and incorporation operational considerations into the decision-making procedure.

1 Introduction

Practitioners of computational materials science know well the figure in which computational techniques and methodologies are plotted against the time and length scales for which they are typically deemed to be appropriate. This figure, reproduced in figure 1A is known by practitioners to provide a qualitative understanding of the overlapping domains of the respective methodologies, implying a continuum of models that offer various strengths and weaknesses for addressing specify types of materials modeling problems. While open to some interpretation, figures such as these are meant to illustrate a broad range of phenomena that can be captured, with each method achieving its own balance between *ab initio* calculation and empirical modeling.

Indeed, our early work modeling of more complex phenomena within lattice-based kinetic Monte Carlo (KMC) atomistic simulations (figure 1B) is one example of attaining such a balance through empirically designed liquid local neighborhoods calibrated alongside analytical continuum models. This balance allowed us to simulate mesoscale, multi-phase phenomena, capturing the evolution of nano- to micrometer features of materials synthesized over a simulated period of 10^{-1} to 10^1 seconds. With such models, we were able to simulate nanoring formation and predict core-shell quantum dot structures in nanomaterials grown via Molecular Beam Epitaxy [1–3], study kinking and faceting phenomenon in nanowire Vapor-Liquid-Solid (VLS) and Vapor-Solid-Solid (VSS) synthesis, and study the evolution of porous material under high-temperature annealing [4]. Through the proper modeling of relevant problem-specific features encompassing a spectrum of atomistic and continuum treatments, we could better capture physical phenomena leading to more insightful simulations at the scales of interest.

Recently, materials science has seen an influx of machine-learning (ML) methods to gain similar insight using data-driven statistical models rather than physical ones. Such methods allow us to

*kreyes3@buffalo.edu

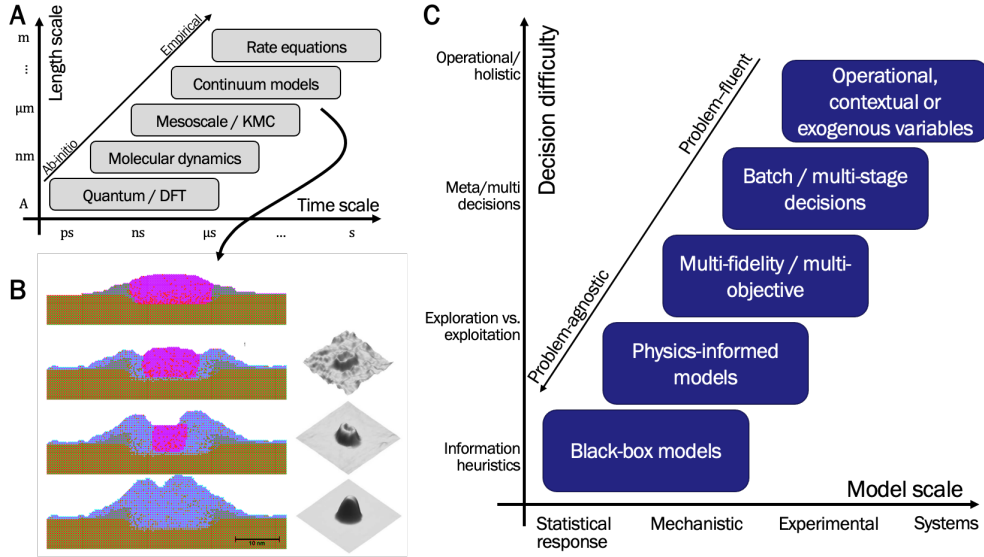


Figure 1: A) Scale comparison of methods from traditional computational materials. B) Example of multi-phase kinetic Monte Carlo simulations of quantum dot formation (taken from [1]). C) An analogous scale comparison for autonomous materials research systems.

study and predict material structure and properties, analyze complex and rich data from materials experiments and even perform autonomous, closed-loop research to design and discover optimal or new materials. Due to the computational nature of such ML techniques, which often require high-performance computing to build, train, and use such models, their application to materials science problems should qualify as a nascent budding branch of computational materials science.

Part of the attractiveness of many ML algorithms is their general-purpose nature. Given a large enough data set, it often suffices to treat any ML-enabled materials science task as the curation of yet-another-data set to train and subsequently apply problem-agnostic models and methods to make predictions, perform materials screening, or analyze data. Yet this problem-agnostic perspective fails to capture the richness of the structure of many materials science tasks. For example, the data requirements of many ML methods, such as deep learning models that often require tens-of-thousands to millions of data points, may be prohibitively too large in a setting where such data must be obtained through laborious, error-prone, and time-intensive physical or computational experiments. As another example, much of the data may be explained through mechanistic physical models that, if utilized correctly, could offset such ostensibly large data requirements. Indeed, such a problem-agnostic, purely data-centric perspective of the application of ML to materials science is analogous to empirical phenomenological models in traditional computational materials science. Extending this analogy, we argue that, like the continuum between *ab initio* and empirical methods of traditional computational materials, the use of ML models and methods have a similar balance between generic, problem agnosticism and more problem-fluent models that are aware of the many subtleties of the materials problem at hand.

This is particularly important in the area of autonomous materials research. This field has garnered recent attention due to the demonstration of several autonomous robotic materials development platforms [5–10]. In such systems, the robot iteratively and efficiently builds knowledge of a material system through strategically selected experiments, the results of which inform the selection of subsequent experiments. While many of these initial systems demonstrate proofs-of-concept using generic, off-the-shelf models and decision-making strategies, this field is primed to further ex-

plore problem-aware modeling. The hope in developing such modeling is to increase the efficiency of autonomous research campaigns and provide the autonomous system more agency in making many higher-order decisions, which are often ignored in the proof-of-concept systems currently in production.

The development of such models and decision-making techniques is depicted in figure 1C. The figure illustrate the breadth of problem-fluency as a function of an autonomous platform’s models of a material system (including what constitutes the “system” itself), along with the considerations it makes when deciding experiments to run. In the lower-left corner, such platforms use empirical, black-box models of experimental responses and make decisions through simple heuristics such as randomized or space-filling designs. At the next level, models incorporate more sophisticated features such as uncertainty quantification and the use of, or inference on physics-based knowledge. With such models, autonomous agents may make correspondingly more complex decisions, including balancing between a) resolving uncertainties of the models or inferring a better understanding of physical mechanisms underpinning observed responses and b) selecting experiments that achieve experimental objectives based on best estimates – this is the *Exploration vs. Exploitation Dilemma* that we outline below.

At the next level, models include multiple aspects of running an experiment such as a) joint models for multi-modal materials characterizations that may be performed on a sample, b) the ability to run physics simulations, and c) a quantification of the fidelities from various measurements that can be made, either *in silico* or physically. This more fluent understanding grants an autonomous platform further agency when making decisions. For example various “multi-” methods such as multi-objective optimization [11–13], multi-fidelity models [14], and multi-information source [15,16] techniques allow agents to not only choose experimental inputs such as synthesis parameters, but also modes of characterization or evaluation, such as choosing to run an experiment versus a simulation and, if tunable, at which fidelity level to run such simulations.

Finally, at the last tier models include more operational or systems-level aspects of running an entire experimental campaign. For example, we can consider modeling a) experimental costs, b) personnel, material or equipment availability, or c) the ability to run campaigns within a heterogeneous network of manual, semi-autonomous and fully autonomous materials experimental apparatuses. With a high-level perspective of experimental campaigns, the decisions that an agent may make here encompass several scales, from deciding individual synthesis conditions that affect a material at the nanoscale, to broad resource allocation decisions that impact the efficiency or success of an entire research campaign.

Through this delineation, we wish to make explicit the analogy with the continuum of models and algorithms from traditional computational materials. As in the choice between empirical and *ab initio* methods, the choice between black-box methods to more problem-fluent ones comes with a trade-off in model simplicity and ease of computation. However, unlike more traditional computational materials, this continuum of autonomous materials techniques as not been explored much. Research in this exploration could result in better modeling and decision-making, allowing us to build more holistic autonomous materials platforms that can achieve accelerated materials design and discovery.

In this article, we review some of our recent progress in this direction. In section 2, we first review the generic framework work we use to model closed-loop autonomous materials research using Bayesian statistics and decision-making policies. We then highlight in section 3 a few examples of our collaborations developing robotic autonomous materials research platforms to illustrate what is possible using only generic, off-the-shelf models and methods. We then introduce examples of integrating problem-specific structure and fluency in both the modeling and decision-making employed by such autonomous research systems. These examples are described in detail in section

4, and include a) the inclusion of physics-based models in concert with ML models and decision-policies, b) the incorporation of more complex decision-making structure to better capture typical decisions made in materials science research, and c) the introduction of operational considerations such as time and costs often encountered when running physical experimental campaigns.

2 Closed-loop design and Autonomous Materials Development

Here we review the basic framework we use for closed-loop autonomous materials development. We use a combination of Bayesian statistical models to represent beliefs about the material systems and use algorithms that select one or more experiments to run based on those beliefs. Experimental observations or responses are then used to update the models, closing the loop. This loop is repeated several times throughout an experimental campaign until some termination criteria are satisfied. Throughout, we usually speak of running an experiment or performing some experimental action. Typically, this means performing an actual physical experiment, though this could also mean running a computer simulation or evaluating some surrogate model of the experiment.

What we present here, which we will call generically “closed-loop design”, has significant overlaps with many models and techniques, which we review in broad strokes. The field of Optimal Experimental Design (OED) considers the selection of experiments with optimal information content, through various definitions of optimality [17, 18]. Active Learning (AL) [19–21], Optimal Learning (OL) [22–24], and Bayesian Optimization (BO) [25, 26] frame the question of informationally optimal experiments within an iterative loop, with each technique using different models representing the system under study and different decision-making policies geared for various experimental objectives. For example, AL is often concerned with reducing uncertainty, while BO and OL policies are geared toward optimizing experimental responses. BO is also used as a global optimization algorithm [27–29], occupying a similar niche as methods like genetic algorithms [30, 31]. Optimal Control (OC) [32, 33] considers the problem of driving a system to a specific state, usually under the assumption of known dynamics. Reinforcement Learning (RL) [34, 35] considers a similar state-dependent control problem, but where some aspect of the dynamics or the effect on the dynamics upon taking some action must be learned through optimally selected actions and closed-loop feedback is obtained through incremental rewards. Such techniques overlap in their modeling of the system being queried, the design of actions and experiments to work toward some objective, and the ability to receive feedback from such actions.

2.1 Basic Formalization

Our approach to closed-loop materials design and autonomous materials development consists of a few basic ingredients, illustrated in figure 2A. We first assume some parameterization of an action or experiment, \mathbf{x} . Upon taking action (such as running an experiment), we assume an experimental response or observation of the form

$$\hat{f}(\mathbf{x}) = f^*(\mathbf{x}) + W. \tag{1}$$

Here we have written the observed response $\hat{f}(\mathbf{x})$ is a random, noisy perturbation of the ground-truth response function $f^*(\mathbf{x})$. Sometimes, we assume some notion of the state S of the experimental campaign, and may sometimes write the ground-truth response as additionally a function of the state: $f^*(\mathbf{x}) = f^*(\mathbf{x}; S)$. We also model some unknown quantities θ^* of the system being studied. This unknown could directly be the ground truth response itself $\theta^* = f^*$ but can represent other unknowns of the system. For example, we could presume that the response may be mechanistically

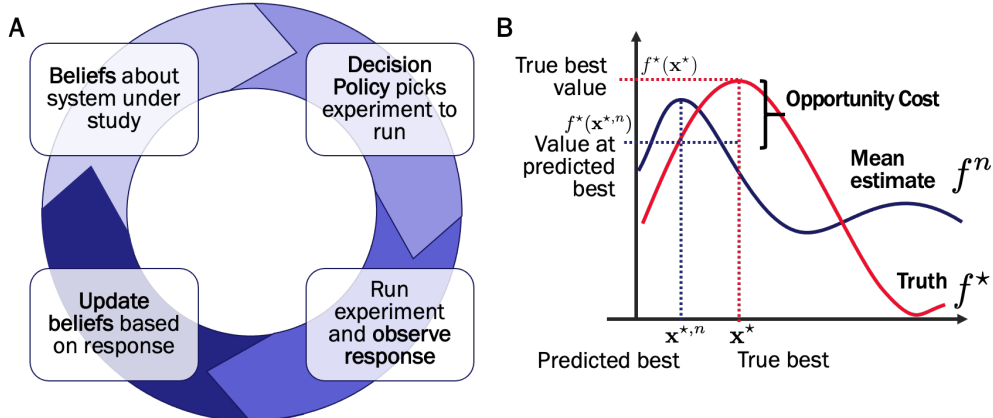


Figure 2: A) A schematic of the closed-loop design main loop employed by several autonomous materials research platforms. B) An illustration of a key metric known as Opportunity Cost used to assess the performance of decision-making policies and models.

or empirically captured using some parameterized forward model $f^*(\mathbf{x}) = f_M(\mathbf{x}; \boldsymbol{\theta}^*)$, in which the unknown quantities represent the effective true value of such parameters.

We assume that if we knew the unknown quantities $\boldsymbol{\theta}^*$ perfectly, we would not have to run any additional experiments. That is, perfect knowledge of these quantities would be all that is needed to compute experimental responses *in silico*, to a high degree of fidelity. However, estimates of $\boldsymbol{\theta}^*$ must be derived from a finite and often limited set of imperfect experimental observations. As such, we never truly have perfect knowledge of the unknown quantities, even having completed several experiments. Instead, knowledge of these unknowns will be modeled to capture such uncertainty. For this, we rely on a Bayesian interpretation: we view the unknowns $\boldsymbol{\theta}^*$ probabilistically, as Random Variables (RVs). Rather than provide a point estimate of what we believe the unknowns to be at any particular stage of an experimental campaign, we instead assign the RVs an entire probability distribution, which captures our uncertain beliefs about the true values of $\boldsymbol{\theta}^*$. Upon receiving additional data, we may update these beliefs to reflect a combination of this new data along with what was believed before this data was observed. This combination results in a posterior belief that blends priors with data in a rigorous way [36]. This Bayesian update is what “closes” the loop in closed-loop autonomous materials research. Depending on the distribution selected to represent the beliefs on $\boldsymbol{\theta}^*$ as well as what is directly observed, performing this Bayesian update could be as easy as evaluating some closed-form formula or may require the use of computationally intensive Monte Carlo methods such as Markov Chain Monte Carlo [37, 38].

The random variable interpretation for $\boldsymbol{\theta}^*$ captures a variety of perspectives for what is deemed to be unknown. If $\boldsymbol{\theta}^*$ represents a finite set of quantities, such as unknown effective parameters to a model, then Bayesian beliefs can be captured through multivariate probability distributions. If $\boldsymbol{\theta}^*$ represents some unknown function, such as in the case where we directly represent beliefs of the ground-truth response function $\boldsymbol{\theta}^* = f^*$, then Bayesian beliefs are probability distributions on random functions, i.e. stochastic processes. For example, perhaps one of the most popular ways of directly representing some experimental response f^* as a function of experimental inputs is with Gaussian Process (GP) beliefs [39, 40], which we denote as

$$f^* \sim \mathcal{GP}(\mu(\mathbf{x}), \Sigma(\mathbf{x}, \mathbf{x}')).$$

This is the functional or infinite-dimensional analog of a multivariate normal (MVN) distribution, and like the MVN distribution, it is parameterized by a mean or expected estimate $\mu(\mathbf{x})$ of

the unknown function $f^*(\mathbf{x})$, along with covariance information captured by the bivariate function $\Sigma(\mathbf{x}, \mathbf{x}')$. The covariance function contains information that qualifies the estimate provided by $\mu(\mathbf{x})$. For example, the diagonal terms $\sigma^2(\mathbf{x}, \mathbf{x}) = \Sigma(\mathbf{x}, \mathbf{x})$ specify the uncertainty associated to the estimate of the unknown function $\mu(\mathbf{x})$ for any particular input \mathbf{x} , while off-diagonal terms $\Sigma(\mathbf{x}, \mathbf{x}')$ describe the assumed statistical relationship between the unknown function values $f^*(\mathbf{x})$ and $f^*(\mathbf{x}')$.

Decision-making policies select the next action to take, given beliefs about the unknown quantities θ^* . These policies typically consider several factors when making such a decision, including — among other considerations — the overall goal or objective of running the closed-loop campaign, what we know about θ^* , and the inherent variability of any response we would observe upon taking the decided-upon action. Due to uncertainties in our beliefs, most policies acknowledge the imperfect and uncertain context in which they are asked to make decisions and often balance between generally resolving uncertainties (called exploration) and focusing on achieving the experimental objectives (called exploitation). Achieving a harmonious balance between exploration versus exploitation leads to an efficient, strategic, and intelligent exploration of experiment space. The unknown quantities are learned to the minimal level of fidelity needed to achieve the goals of a campaign.

Two typical objectives are 1) *response optimization* and 2) *global learning*. In response optimization, the task is to identify the input \mathbf{x}^* whose resulting response is, on average, optimal over the entire space of feasible inputs \mathcal{X} . In symbols, we wish to learn

$$x^* = \max_{x \in \mathcal{X}} f^*(x),$$

In global learning, the objective learns the unknown quantities outright, i.e., learn the most accurate estimate of θ^* . This could mean, as examples, learning the response surface if $\theta^* = f^*$ or learning the effective parameters to a physics-based model. Specific policies are meant for specific experimental objectives. For example, in response optimization, two policies we often use in our own work are the Knowledge Gradient (KG) policy [41, 42] and Expected Improvement (EI) policy [43, 44], both of which are examples of Look-Ahead policies. Such policies attempt to estimate the expected impact of running a potential experiment on future, posterior beliefs, using current beliefs to calculate this expectation. Policies for global learning include many of the so-called Alphabet-optimality designs [45] and many active learning strategies.

While we have described the basic and generic framework for closed-loop design, we shall see that the implementation of the different components varies significantly in model and algorithm complexity and the ability to capture the specific structure of a problem. We will highlight a few examples of this in section 4. However, due to the ubiquity of the generic problem of iterative decision-making under uncertainty, many off-the-shelf techniques have been developed that can be applied directly to autonomous materials research platforms to perform, to first order, basic decision-making to optimize material properties. In the next section, we will review some of our collaborative work in developing such autonomous systems.

3 Examples of closed-loop autonomous materials platforms

This generic framework encompasses many closed-loop or active learning scenarios in which Bayesian beliefs are interactively improved, and experimental objectives are pursued in tandem. One of the most popular forms of such closed-looped methods is black-box Bayesian optimization (BO). In black-box BO, beliefs on the response function are typically directly represented by GPs or other

types of statistical or machine learning models, and policies such as EI are used to select information-rich experiments to identify the experimental inputs that optimize the observed response in as few iterations around the closed-loop as possible. Much of our work in BO has been implementing and adapting such methods within the context of autonomous materials systems.

For example, with Keith Brown at Boston University, we have applied this black-box BO framework in optimizing mechanical properties of additively manufactured mechanical structures using a Bayesian autonomous researcher (BEAR) that consisted of an array of 3D printers, a robot arm, and mechanical testing equipment [9]. Using GP beliefs models of structure toughness in tandem with the EI policy, we had shown how the autonomous system efficiently explores a four-dimensional parameterized structure space to identify those structures that optimized certain mechanical properties, resulting in an almost 60 times reduction in the number of structures tested when compared to a traditional factorial design of experiments.

In another collaboration, with Milad Abolhasani at North Carolina State University, we studied the use of an ensemble of models to represent beliefs on experimental response functions to optimize properties of colloidal quantum dots (QDs) synthesized by an autonomous flow reactor, the Artificial Chemist [8]. Rather than capture a continuous space of response functions using a distribution on functions, as with GPs, ensemble beliefs use a finite sample of potential candidate response functions. Summary statistics, such as expected values or covariances, typically calculated using a distribution like a GPs, can be approximated using sample statistics over the ensemble. Ensemble beliefs also allow for the use of more complex models, which in the Artificial Chemist case consisted of ensembles of neural networks. Using the autonomous Artificial Chemist and a variety of BO-oriented policies, we studied the effectiveness of this model and policies to quickly tune properties of flow-reactor synthesized colloidal QD.

These and other examples point to the opportunities that even generic, off-the-shelf models and algorithms such as GPs and EI can help accelerate materials research through an intelligent and strategic exploration of design space. Techniques and models such as GP beliefs and the EI decision-making policy for black-box BO are generic. The same models and methods have found popular applications elsewhere, apart from autonomous materials research. For example, BO has experienced recent popularity as a global-optimization method used to tune hyper-parameters of ML models [25, 27, 46] In this application, hyper-parameter space is iteratively explored, and different hyper-parameters are evaluated through an objective function such as an error on validation or hold-out data sets. Finding a global optimum of such an objective function could result in optimally calibrated and validated models.

However, this example betrays one reason why we may wish to consider models and methods beyond black-box BO for autonomous materials design. In contrast to evaluating validation errors for some ML model, which is all done *in silico*, using generic BO methods in materials research ignores many realistic aspects of running **actual, physical experiments** that, as we show in the sequel, contribute significantly to the overall success and efficiency of any closed-loop autonomous experimental campaign. For example, in addition to information-theoretic considerations typically considered in decision-making policies, we ought to make other, more operational or problem-specific ones when selecting experiments to run. In contrast to hyperparameter optimization, where there is no additional cost incurred when selecting vastly different parameters in succession, physical experiments often do incur such a penalty, such as different times required to increase versus decrease temperature of a furnace, or the cost of selecting one type of catalyst material versus another, or the effort and time needed to select one characterization method versus another. Often, the time to run an experiment, wait for a system to equilibrate, or wait for mechanical failure to occur must be decided as well, and many off-the-shelf models and methods do not elegantly incorporate this. Much of our work focuses on modeling such aspects of running

physical experiments as rigorously as possible. In the next section, we focus on three examples of such modeling.

4 Higher features of materials experiments

In developing more problem-fluent closed-loop autonomous materials platforms, we have focused on better modeling problem-specific structure and prior knowledge, and decision-making methods that better integrate operational costs and rewards. Below, we list a few such methods and extensions we have employed in the past.

4.1 Incorporating physical models

Perhaps one of the most striking departures we may take away from generic, off-the-shelf closed-loop techniques such as black-box BO is the ability to hypothesize or otherwise specify physics-based, mechanistic insight relating the experimental actions with observed experimental responses. By including physical models, we can impose a more-specific structure on our predictions of response surfaces or other unknown quantities, in contrast to the generic continuity or smoothness assumptions that come equipped with purely statistical models such as GPs. By integrating these models with Bayesian techniques, we can additionally provide the qualification needed on such prediction to reflect uncertainties arising due to model inaccuracies and noisy data. Such an uncertainty quantification of predictions derived from a physics-based model could subsequently inform decision-making policies to select the next experiment. Such hybrid physical/statistical models and decision-making that use them reside the box labeled “Physics-informed models” from the left in figure 1C.

One example of using physical models in the decision-making closed loop is presented in [47]. Here, we performed a simulation study in which we considered the optimization of synthesis and processing conditions to create a nanoemulsion. These conditions were optimized against a measure of the stability of such an emulsion, capturing two aspects. First, we desired the synthesized emulsion to exhibit long-term stability at room temperature. Second, we required the emulsion to be effectively destabilized at a high temperature. An emulsion satisfying both criteria could be used to deliver payload molecules contained in such an emulsion in a controlled, thermally activated fashion.

In [47], we derived a kinetic model based on a system of ordinary differential equations describing the destabilization of such an emulsion, writing the objective experimental response function in terms of controls, here the synthesis and processing conditions, and a few effective physical parameters to the model, including energy barriers and rate prefactors determining the kinetics of emulsion instability $f_M(\mathbf{x}; \boldsymbol{\theta})$. Under the assumption that the model reflected the physical truth, up to the true value of the effective physical parameters $\boldsymbol{\theta}^*$, we imposed Bayesian beliefs on these parameters through a finite sample of L candidate parameter values $\Theta = \{\boldsymbol{\theta}_1, \dots, \boldsymbol{\theta}_L\}$. This discretization of physical parameter space affords us simplicity in approaching the Bayesian statistical calculations, effectively turning the problem of assigning Bayesian beliefs into one of Bayesian hypothesis testing [48, 49], with each of the L candidate parameter values severing as a hypothesis of what the unknown, ground-truth parameter values are. At any point throughout the campaign, we maintain the probabilities that each candidate is indeed the ground-truth

$$p_i = \mathbb{P}[\boldsymbol{\theta}^* = \boldsymbol{\theta}_i]$$

As new data is received, Bayes’s law tells us how to update these probabilities.

These probabilities along with the physical model of the response $f_M(\mathbf{x}; \boldsymbol{\theta})$ also provide a sample of candidate, mechanistic forward models $f_i = f_M(\mathbf{x}; \boldsymbol{\theta}_i)$, each qualified with the probabilities p_i

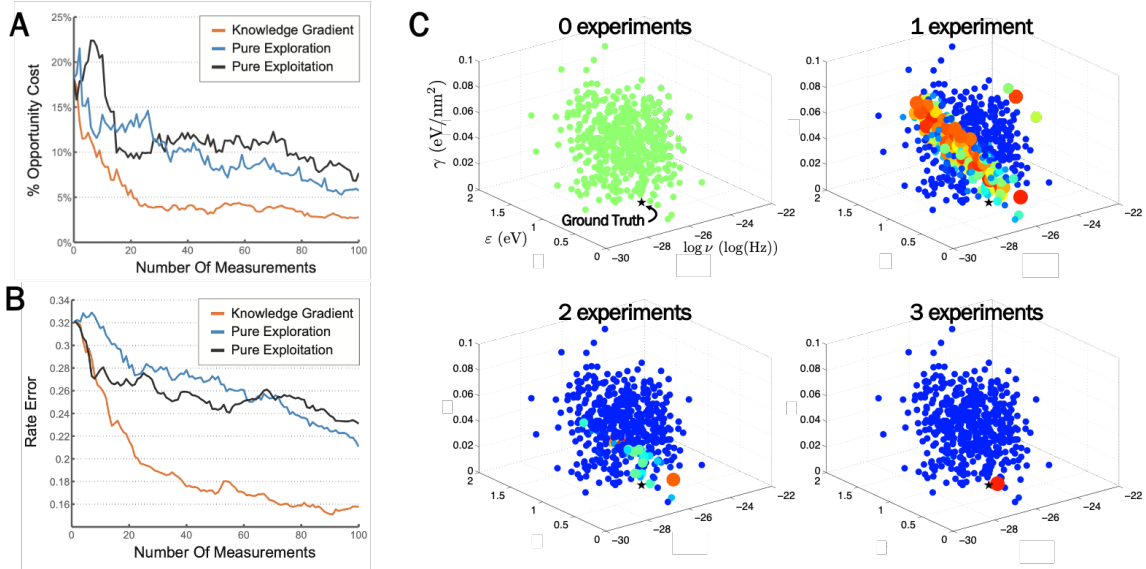


Figure 3: *A) Percent opportunity cost and B) coalescence rate estimation error versus number of experiments for KG and baseline policies, from [47]. C) Evolving Bayesian beliefs on physical parameters. Each dot is a sample of three physical parameters to a kinetic model: an interfacial energy γ , an activation energy ϵ and a reaction rate prefactor ν . Larger, redder points correspond to higher posterior probabilities, while smaller, bluer points indicate smaller posterior probabilities.*

that they represent the ground-truth, unknown response $f^*(\mathbf{x}) = f_m(\mathbf{x}; \theta^*)$. This sample set of candidates, along with probabilities representing Bayesian beliefs on such candidate, is a type of Bayesian Model Averaging (BMA) [50]. With BMA, we can utilize physical models within a Bayesian setting. With such BMA-based beliefs, we use the Knowledge Gradient (KG) decision policy, which selects the experiment \mathbf{x} — here a set of synthesis conditions — that maximize the expectation

$$\nu_{\text{KG}}(\mathbf{x}) = \mathbb{E} \left[\max_{\mathbf{x}'} f^{n+1}(\mathbf{x}') - \max_{\mathbf{x}'} f^n(\mathbf{x}') \right] \quad (2)$$

where f^n is the current mean-estimate of the response and f^{n+1} is the future mean-estimate of the response if we were to run experiment \mathbf{x} and the expectation is the weighted average over the potential response outcomes of such an experiment. This expectation is sometimes called an acquisition function, and different such functions define other policies.

We run simulations to show how effective a closed-loop campaign that uses both the BMA beliefs and the KG decision-policy is in finding the synthesis conditions that optimize the response. This is plotted in figure 3A, which plots a performance metric called percent Opportunity Cost (OC, figure 2B), calculated and averaged over several simulations, where simulations sampled different ground-truth values of parameters θ^* . OC reflects how much better the true optimal expected response value is compared to the expected response value for the experiment believed to be optimal, reflecting a penalty we pay for not picking the true optimal experimental conditions. Lower OC indicates better performance in identifying optimal or near-optimal synthesis conditions. We also compared the KG policy against baseline policies. Compared to such policies, the KG policy was significantly more effective in identifying the optimal set of synthesis conditions over various ground truth scenarios.

Because of our use of parameterized physics models, the candidate parameters θ_i along with the probabilities p_i allow us to calculate weighted averaged estimates of the effective parameter

values $\theta^* \approx \sum_{i=1}^L \theta_i p_i$. As such, the evolving probabilities obtained after successive iterations of the closed-loop provide increasingly refined insight regarding the physical processes underpinning the observed experimental responses. For example, in figure 3B, we plot the error of the mean estimate of the droplet coalescence rate, which is a key kinetic process contributing to emulsion stability. This error is a comparison between the rate as determined by the averaged estimate $\sum_i \theta_i p_i$ of the kinetic parameters and the true-rate calculated from the ground-truth parameter values θ^* , averaged over all simulations performed. We see that, in comparison to the baseline policies, KG more efficiently learns the rate of this process.

The use of physics-based models, when coupled with BMA and policies such as KG, show the promise of deriving physical insight while simultaneously optimizing material properties or experimental responses. This insight becomes more effective if the set of candidates is selected to represent a diverse set of models and mechanistic explanations of what could potentially contribute to the observable response. How to optimally generate and hypothesize such a set of models is an open topic of research, and is a subject of some of our recent work. In [51], we specifically address two major points of concern with the above BMA model. First is the assumption of a globally applicable physical model $f_M(\mathbf{x}, \theta)$. We explore the mixture of physics-based models with statistical ones such as a GPs through the use of local semi-parametric models, combine together through a Gaussian kernel. In this way, we can consider fitting reduced-order local models individually for smaller regions of experiment space \mathcal{X} . Such models may, for example, encompass a smaller set of physical processes than a global model.

The second point addressed in [51] is selecting models to include in the set Θ of candidate models. One typically encountered phenomenon when using BMA is the apparent dominance of one candidate after a small number of observations [52]. This is illustrated in figure 3C, which visualizes BMA beliefs on three-dimensional physical parameter space of a simplified kinetic model derived from that used in [47]. Here the three physical parameters describe an interfacial energy γ , an activation energy ε , and a reaction rate prefactor ν . Each point in the figure represents a single candidate parameter vector $\theta_i = (\gamma_i, \varepsilon_i, \log \nu_i)$, while the star represents the ground truth parameter. The sizes and colors assigned to each point indicate the probabilities p_i , with larger, redder points representing larger probabilities, and smaller, bluer points representing smaller ones. The figure shows the evolution of beliefs after performing experiments selected using the KG policy. After three data-points, one choice of parameters, hence one model dominates — the posterior probability associated with it is effectively 1. In contrast, the other parameters have a corresponding posterior probability of 0. While not exactly correct, the dominant parameter is relatively close to the true parameter values. This represents a coarse-grain refinement of our beliefs to identify a promising region in parameter space. This identification allows us to resample a new set of parameters effectively. Here we face several decisions regarding how to perform such a resampling. For example, should we include models only in the local neighborhood of the dominant model, or should we appreciate the fact that this model is dominant in the face of a small number of noisy data points? In [51], we attempt to address such questions and develop algorithms for coarse-grained and fine-grained refinement of the set of candidate models in the face of such model uncertainty.

In summary, within a Bayesian context, we can utilize knowledge about physical, mechanistic models that predict responses we observe experimentally. Such a hybrid physical / Bayesian models can then be used with decision-making policies to select experiments that balance between exploration and exploitation. Due to our use of physics models, exploration amounts to more than resolving statistical uncertainties, which is the case when using black-box empirical models such as GPs, placing the technique one level removed from the most empirical methods outlined in figure 1C. Instead, we can perform inference about the true mechanisms underpinning observed

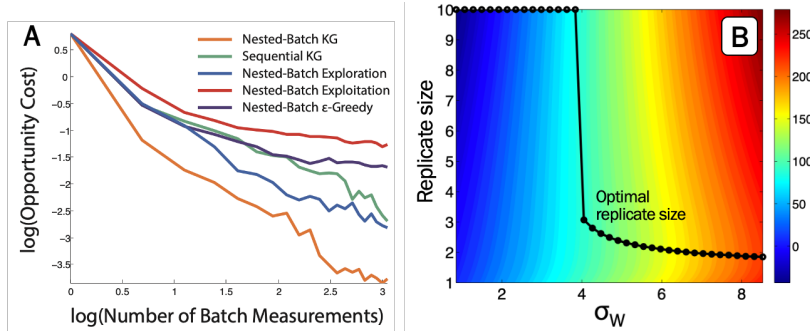


Figure 4: A) Opportunity cost versus number of experiments for nested-batch mode policies, taken from [53]. B) Total cost (color value) versus single-period noise standard deviation and number of replicates, and the optimal replicate size (black circles and lines) for a given noise level, taken from [54].

responses. In this way, we can use such a campaign to optimize synthesis conditions while simultaneously learning about the physics of the material system under study.

4.2 Decision structure and meta-decisions in materials experiments

Another form of problem-specific structure considers how decisions are made and additional meta-decisions that impact an experimental campaign. In [53], we explore the problem of optimizing the output current of an optoelectronic device created by attaching nanoparticles to a photosensitive substrate. The design variables are the size, shape, and composition of the nanoparticles, in addition to the density of the nanoparticles on the substrate. While finding the optimal design variables that maximize output current could be addressed using problem-agnostic BO methods and algorithms, such a solution disregards the fact that the nanoparticles take time to synthesize. Also, nanoparticle density can be varied in a high-throughput manner by depositing NPs with a density gradient on the substrate. As such, it is costly to vary the size, shape, and composition of the NPs, but several NP densities can be tested simultaneously and in parallel. Such a problem would occupy the space between the boxes labeled “Batch / multi-stage decisions” and “Operational, contextual, or exogenous variables” in figure 1C due to the consideration of experimental structure, and the operational constraints such structure poses.

This imposes a nested and batched structure to the decisions. First, we must decide on a specific nanoparticle type by specifying shape, size, and composition. Once synthesized, we may consider a batch of NP densities as a second, nested decision. In [53], we showed how to augment current BO policies, such as the KG policy, to incorporate this nested-batch decision-making structure. This is done through a simulation-optimization procedure that used Monte Carlo simulations to sample and select design parameters over which to compute the expectation needed to calculate the KG acquisition function value defined in equation (2). Figure 4A shows simulation results comparing nested-batch KG policy with other baseline policies, showing the augmented nested-batch KG policy outperforming the KG policy that does not properly model the nested-batch nature of the decisions being made, and nested-batched versions of other baseline policies.

As illustrated above, the cost of running any particular experiment is a reality of physical experimentation that is not properly modeled using normal closed-loop design methods such as BO. In [54] we explore this further through an analysis of meta-decisions made in an experiment and the costs associated with such decisions. We consider archetypal experimental design meta-decisions such as the number of experiment replicates performed, such as performing experiments in duplicate or triplicate. By averaging the responses of such an ensemble of near-identical experiments,

scientists hope to reduce the impact of noise. In fact, if we assume an experimental response is perturbed through an additive Gaussian noise as in equation (1), then assuming this noise has variance σ_W^2 , the averaged response over n independent replicates of the experiment should have a reduced variance of σ_W^2/n . However, this replication comes at an experimental cost, which depends on the parallelizability available to run such an n -fold replicated study. If done sequentially, the effectively reduced variance is obtained with a factor of n additional experiments. In contrast, perfectly parallel experiments do not incur any additional experimental cost compared to running a single experiment. This cost of running n experiments can be captured through the formula

$$C_\alpha(n) = \alpha + (1 - \alpha) \cdot n$$

where α is a number between 0 and 1 that serves as a measure of parallelizability. In [54], we consider the impact of a campaign’s total cost with respect to this and other hyper-parameters such as measurement noise and campaign stopping criteria. For example, in 4B, we plot the total cost of a campaign needed to find reduce the opportunity cost to within 7%, assuming a parallelizability coefficient $\alpha = 0.6$ using the KG policy. This total cost of a campaign is plotted with respect to the single-experiment noise σ_W and the replicate size n .

The black dots and connecting lines indicate the optimal replicate size for any given amount of noise. This is the replicate size that minimizes the total cost of the campaign. Counter-intuitively, these simulations show that for this problem, as the single-experiment noise becomes larger, it is advantageous to select a smaller number of identical experiments per each iteration of the closed-loop campaign. One way to understand this result is to acknowledge that the KG policy often performs relatively better in high-noise scenarios than other policies. Reducing the replicate size to 1 simply in such scenarios allows the KG policy to be more agile in adaptively selecting n different experiments rather than n identical experiments for this amount of parallelization.

4.3 State of the campaign and operational considerations

The last example of problem-specific structure considers the case of operational considerations of running an experimental campaign. Such considerations allow us to consider and optimally select operational variables that impact some notion of reward or costs of an experiment and consider the campaign’s termination criteria based on such costs. One common example of such considerations and termination criteria is the time to perform a particular experiment and the overall time-budget of a campaign. Another example is considering the probability of failure in running an experiment. Very often, such costs and termination constraints depend on maintaining a more complicated nature of the state, apart from the simple state-of-belief that we have used thus far. For example, if we are concerned about a fixed time-budget for running an autonomous experimental campaign, then we must consider how long we have spent in the current campaign whenever we decide on the next action. Problems concerning this and other operational considerations would fall in the top-right box of figure 1C.

Here, we employ the generic framework of Reinforcement Learning (RL) and Markov Decision Processes (MDPs), which is not a large departure from the one presented in section 2. The main differences here is the notion of the state of a campaign, a criterion to determine when a campaign is terminal and should be stopped, and the formulation of the decision-policy based on some measure $R(S, \mathbf{x}, y)$ of the rewards obtained or costs — sometimes called regret — incurred after taking a particular action \mathbf{x} from a particular state S and observing a specific outcome y . Given a sequence of states, $\{S_i\}$ actions taken by such states according to some decision-making policy $\{\mathbf{x}_i = \pi(S_i)\}$ and the resultant experimental outcomes from such actions $\{y_i\}$, we can define the total cumulative

reward

$$\sum_i R(S_i, \mathbf{x}_i, y_i),$$

One of the goals in reinforcement learning is to select the \mathbf{x}_i , i.e., learn the policy that maximizes this total cumulative reward on average. Key to this is the concept of the value of a state $V^\pi(S)$, which we may think of as the total additional rewards we can expect to obtain starting from this state S and proceeding with our experimental campaign using policy π until we arrive at some terminal state. Thus, like KG and EI, the value of a state is the expectation of some future quantity that measures the quality of a particular state. However, unlike KG and EI, the value V^π considers modeling not only the outcome of a single future experiment but the outcome of an entire experimental campaign. It is computationally infeasible to calculate such values exactly, and many RL techniques such as value-function iteration, policy-function iteration [34, 55] and Q-learning [56], are essentially centered around approximating this or other related functions. The result is an approximation of **the** optimal policy, i.e. the one geared toward maximizing cumulative reward or minimizing cumulative regret.

Under this framework, rather than identifying and testing different policies, we instead define different reward structures. This provides a more flexible method for including constraints and operational considerations. For example, if we wished to optimize a material response subject to the constraint that we cannot surpass a particular time-budget for a campaign, we can specify the time-budget as a termination criterion and specify a single reward obtained at the end of a campaign equal to the maximum/minimum of the predicted response overall potential experimental inputs

$$R(S_i, \mathbf{x}_i, y_i) = \begin{cases} \max \mu_{S_i}(\mathbf{x}) & \text{if } S_i \text{ is terminal.} \\ 0 & \text{otherwise.} \end{cases}$$

where $\mu_{S_i}(\mathbf{x})$ is the mean estimate of the response given we are in state S_i .

One method we employ to calculate state values and make decisions within this RL framework is Monte Carlo Tree Search (MCTS). MCTS is a method for sampling experimental campaign scenarios that potentially result in high-value states [57, 58]. This is done through sequentially building up a tree of scenarios that enumerate various simulated experimental decisions, outcomes, and future states. Having such a scenario tree, we can approximate the utility of pursuing any particular branch, which results in a decision-making policy: select the action leading down the branch with the highest expected cumulative rewards. An example scenario tree is depicted in figure 5A. Here the blue vertices denote instances of a simulated decision being made during some simulated experimental campaign. Red vertices reflect the state obtained after making such a decision and obtaining a simulated outcome. The size of the nodes indicates the value associated with a particular state or action. We observe a discrepancy of values for different scenarios, which informs what actions to pursue from the actual current state of the campaign, which is highlighted in the figure.

Such a framework allows us to include more problem-specific operational considerations in our decision-making. For example, we may consider the following scenario, motivated by experiments performed at the Relativistic Heavy Ion Collider at Brookhaven National Laboratory [59]. One such experiment measures the distribution of net-baryon number fluctuations produced as a function of the collider’s beam energy, as part of the Beam Energy Scan program, which is attempting to search for a conjectured critical point of the phase diagram of quantum chromodynamics [60]. In particular, identifying minima and other features of moments of this distribution, such as the kurtosis of the distribution $\kappa(E)$, seen as an experimental response as a function of beam energy E , help scientists in this critical point search [61–63].

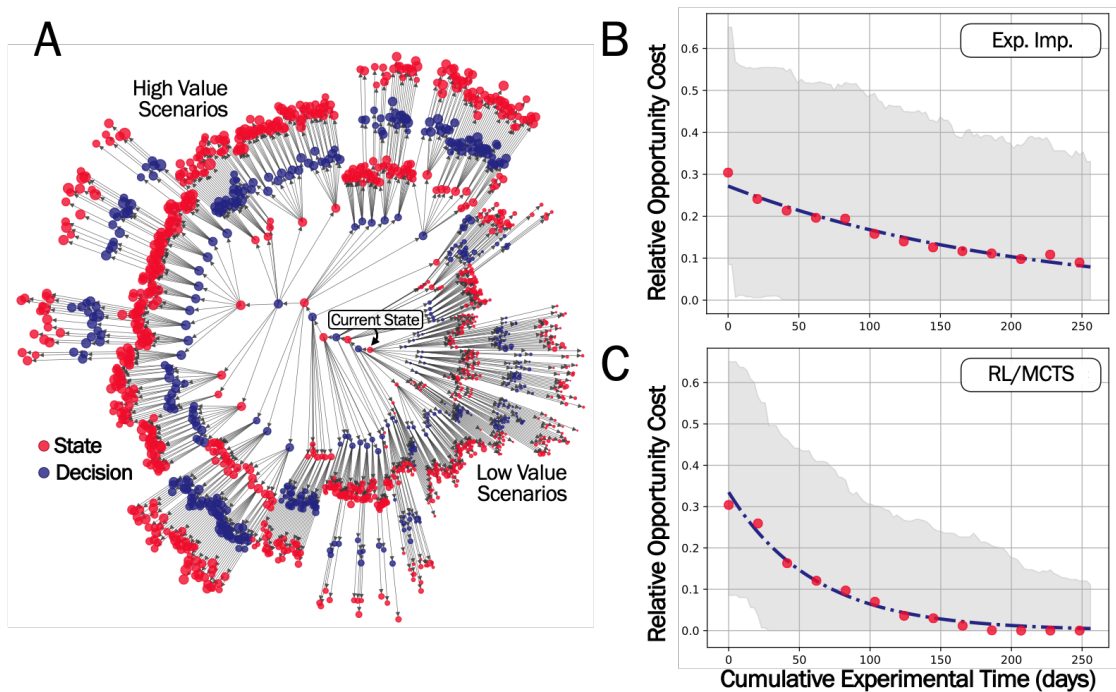


Figure 5: A) A scenario tree sampled using Monte Carlo Tree Search, enumerating high-value future scenarios of an experimental campaign. Red vertices correspond to simulated future states, and blue vertices are simulated future decisions. Vertex size indicates the value assigned to the state or action. B) and C) Opportunity cost versus cumulative experimental time using a BO policy and a MCTS/RL policy, respectively. Red dots indicate median OC values obtained over several simulations, and dotted blue line is an exponential decay fit. Gray regions indicate the envelope between 25th and 75th percentiles of OC values.

Identifying the optimal energy E that minimizes the net-baryon kurtosis response function $\kappa^*(E)$ can be approached using vanilla BO methods. However, such methods do not appropriately appreciate an operational choice of experiment time. That is, scientists at RHIC, in addition to energy, must specify the time. In principle, the ground-truth net-baryon distribution is not impacted by experiment time. However, the observed estimate of this net-baryon distribution does depend on experimental time in addition to energy. This discrepancy between the ground-truth kurtosis $\kappa^*(E)$ and the observed kurtosis can be modeled as heteroscedastic noise, so that we can write the observed kurtosis response $\hat{\kappa}(E, t)$ obtained when running an experiment with beam energy E and experiment time t as

$$\hat{\kappa}(E, t) = \kappa^*(E) + W(E, t)$$

where $W(E, t) \sim \mathcal{N}(0, \sigma_W^2(E, t))$ is Gaussian noise with variance $\sigma_W^2(E, t)$ that depends on E and t . One model assumes that the noise level is inversely proportional to E^3 and t . That is, noise decreases at higher energies and longer experiment times. Thus there is a trade-off between experimental accuracy and experimental time. Proper, problem-fluent policies that appreciate this trade-off will balance selecting a large number of potentially inaccurate experiments versus a small number of accurate experiments. However, vanilla BO policies such as EI do not make such a consideration.

Figure 5B shows the results of several hundred simulated closed-loop BO campaigns run to find optimal energies of sampled ground-truth kurtosis response functions using GP beliefs for κ^* and an EI policy. The figure plots the median, 25th, and 75th percentiles of relative OC as a function of experiment campaign time, rather than the number of experiments. We see that after a simulated campaign time of 256 days, the EI policy can find, on average, energies producing kurtosis response that within 10% of the optimal, minimal kurtosis response. In contrast, by using MCTS-based RL policy, cognizant of the time budget of 256 days, and the above noise model, we obtain the simulation results depicted in figure 5C. Here we see that this RL-policy obtains a similar optimality level in around 80 days, which reflects a campaign speed-up factor of more than 3.

The key difference between BO-based policies and RL-based ones is that BO-policies make information-theoretic considerations designed to minimize the number of iterations around the closed-loop. With RL-based policies, we can add more complex rewards and regrets that reflect additional measures of experimental costs and impose campaign termination constraints that reflect budgets on those costs. Simulations of entire campaigns can use such constraints to more effectively and holistically plan the next experiment with the remaining campaign budget in mind. While the above example of experiments at the RHIC may seem exotic, the general tradeoff between experiment time and accuracy is common throughout experimental science. This trade-off exists when deciding how long to run an experiment to obtain a reasonable, extrapolated estimation of some material property. This could arise when trying to extrapolate a quantity of a material or chemical system at an equilibrated state, such as predicting equilibrium chemical concentrations through the determination of reaction rates. This also arises when extrapolating for out-of-equilibrium or long timescale events and properties, like failure times of a mechanical component. Using RL-based policies, we can better include this trade-off when planning autonomous materials campaigns.

5 Conclusion

We have outlined a few examples of how we have approached closed-loop autonomous materials design through a common framework that involves Bayesian beliefs about the system being studied and decision-making policies that select optimal experimental actions to run. We have shown

examples of how black-box models and methods can accelerate materials research but have indicted three samples of how such techniques are deficient. By integrating problem-specific structure, we showed a few examples of how we rectify such deficiencies.

As ML models and methods become more commonplace in materials science research, we have the opportunity to enrich traditionally data-driven, problem agnostic techniques with problem-specific structure. Doing so in the context of ML for materials could result in smaller data requirements, more robust models, and the ability to draw interpretable scientific insight. This opportunity is well-pronounced in the new area of autonomous materials development, where combining data-driven statistical models with physics and operational considerations result in a more meaningful, scientifically richer autonomous materials exploration in which robot scientists have the agency to pursue and make higher-order decisions and formulate more complex knowledge of the material system being studied.

The idea of combining physical, statistical, and operational models to form a such continuum of methods appropriate at different scales of knowledge and decision-making capabilities (figure 1C) is analogous to the continuum of computational materials methods that straddle length and time scales (figure 1A). As computational material scientists, we understand that no one method is globally appropriate. By understanding the benefits, risks, and trade-offs between models at different scales, we can tackle materials modeling problems more effectively. So too, we believe, can we effectively apply ML and statistical models and methods through an appreciation of their strengths and weaknesses, supplementing the latter with more problem-fluent approaches.

6 Acknowledgments

This review features work resulting from helpful conversations and collaborations with several groups. Specifically, we acknowledge Si Chen, Yan Li, Yingfei Wang, Xinyu He and Warren Powell from Princeton University, Frank Alexander, Kevin Yager, Jaimie Dunlop from Brookhaven National Laboratory, and Benji Maruyama, Rahul Rao, Jennifer Carpena, Ahmad Islam and Pavel Nikolaev from the Air Force Research Laboratory, Keith Brown and Aldair Gongora at Boston University, and Milad Abolhasani and Robert Epps at North Carolina State University.

7 Data Availability

The raw data required to reproduce these findings are available to download from

<https://www.csms.io/data>

The processed data required to reproduce these findings are available to download from

<https://www.csms.io/data>

References

- [1] K. Reyes, P. Smereka, D. Nothorn, J. M. Millunchick, S. Bietti, C. Somaschini, S. Sanguinetti, and C. Frigeri, “Unified model of droplet epitaxy for compound semiconductor nanostructures: experiments and theory,” *Physical Review B*, vol. 87, no. 16, p. 165406, 2013.
- [2] M. DeJarld, K. Reyes, P. Smereka, and J. Millunchick, “Mechanisms of ring and island formation in lattice mismatched droplet epitaxy,” *Applied Physics Letters*, vol. 102, no. 13, p. 133107, 2013.

- [3] M. Bollani, S. Bietti, C. Frigeri, D. Chrastina, K. Reyes, P. Smereka, J. Millunchick, G. M. Vanacore, M. Burghammer, A. Tagliaferri, *et al.*, “Ordered arrays of embedded ga nanoparticles on patterned silicon substrates,” *Nanotechnology*, vol. 25, no. 20, p. 205301, 2014.
- [4] K. Reyes, “Fast kinetic monte carlo simulations using hash table based caching with applications to nanowire growth and sintering,” *SIAM Journal on Multiscale Modeling and Simulation*, vol. 12, no. 1, pp. 200–224, 2014.
- [5] P. Nikolaev, D. Hooper, F. Webber, R. Rao, K. Decker, M. Krein, J. Poleski, R. Barto, and B. Maruyama, “Autonomy in materials research: a case study in carbon nanotube growth,” *npj Computational Materials*, vol. 2, no. 1, pp. 1–6, 2016.
- [6] J. Chang, P. Nikolaev, J. Carpena-Núñez, R. Rao, K. Decker, A. E. Islam, J. Kim, M. A. Pitt, J. I. Myung, and B. Maruyama, “Efficient closed-loop maximization of carbon nanotube growth rate using bayesian optimization,” *Scientific Reports*, vol. 10, no. 1, pp. 1–9, 2020.
- [7] A. G. Kusne, H. Yu, C. Wu, H. Zhang, J. Hattrick-Simpers, B. DeCost, S. Sarker, C. Oses, C. Toher, S. Curtarolo, *et al.*, “On-the-fly closed-loop materials discovery via bayesian active learning,” *Nature communications*, vol. 11, no. 1, pp. 1–11, 2020.
- [8] R. W. Epps, M. S. Bowen, A. A. Volk, K. Abdel-Latif, S. Han, K. G. Reyes, A. Amassian, and M. Abolhasani, “Artificial chemist: An autonomous quantum dot synthesis bot,” *Advanced Materials*, p. 2001626, 2020.
- [9] A. E. Gongora, B. Xu, W. Perry, C. Okoye, P. Riley, K. G. Reyes, E. F. Morgan, and K. A. Brown, “A bayesian experimental autonomous researcher for mechanical design,” *Science Advances*, vol. 6, no. 15, p. eaaz1708, 2020.
- [10] L. M. Roch, F. Häse, C. Kreisbeck, T. Tamayo-Mendoza, L. P. Yunker, J. E. Hein, and A. Aspuru-Guzik, “Chemos: An orchestration software to democratize autonomous discovery,” *PLoS One*, vol. 15, no. 4, p. e0229862, 2020.
- [11] K. Miettinen, *Nonlinear multiobjective optimization*, vol. 12. Springer Science & Business Media, 2012.
- [12] E. Zitzler and L. Thiele, “Multiobjective evolutionary algorithms: a comparative case study and the strength pareto approach,” *IEEE transactions on Evolutionary Computation*, vol. 3, no. 4, pp. 257–271, 1999.
- [13] K. Shimoyama, S. Jeong, and S. Obayashi, “Kriging-surrogate-based optimization considering expected hypervolume improvement in non-constrained many-objective test problems,” in *2013 IEEE Congress on Evolutionary Computation*, pp. 658–665, IEEE, 2013.
- [14] B. Peherstorfer, K. Willcox, and M. Gunzburger, “Survey of multifidelity methods in uncertainty propagation, inference, and optimization,” *Siam Review*, vol. 60, no. 3, pp. 550–591, 2018.
- [15] M. Poloczek, J. Wang, and P. I. Frazier, “Multi-information source optimization,” in *Proceedings of the 31st International Conference on Neural Information Processing Systems*, pp. 4291–4301, 2017.

- [16] R. Lam, D. L. Allaire, and K. E. Willcox, “Multifidelity optimization using statistical surrogate modeling for non-hierarchical information sources,” in *56th AIAA/ASCE/AHS/ASC Structures, Structural Dynamics, and Materials Conference*, p. 0143, 2015.
- [17] R. A. Fisher, “Design of experiments,” *Br Med J*, vol. 1, no. 3923, pp. 554–554, 1936.
- [18] R. W. Kennard and L. A. Stone, “Computer aided design of experiments,” *Technometrics*, vol. 11, no. 1, pp. 137–148, 1969.
- [19] B. Settles, “Active learning literature survey,” tech. rep., University of Wisconsin-Madison Department of Computer Sciences, 2009.
- [20] D. Cohn, L. Atlas, and R. Ladner, “Improving generalization with active learning,” *Machine learning*, vol. 15, no. 2, pp. 201–221, 1994.
- [21] D. A. Cohn, Z. Ghahramani, and M. I. Jordan, “Active learning with statistical models,” *Journal of artificial intelligence research*, vol. 4, pp. 129–145, 1996.
- [22] I. O. Ryzhov, W. B. Powell, and P. I. Frazier, “The knowledge gradient algorithm for a general class of online learning problems,” *Operations Research*, vol. 60, no. 1, pp. 180–195, 2012.
- [23] W. B. Powell and I. O. Ryzhov, *Optimal learning*, vol. 841. John Wiley & Sons, 2012.
- [24] W. B. Powell and P. Frazier, “Optimal learning,” in *State-of-the-Art Decision-Making Tools in the Information-Intensive Age*, pp. 213–246, Informs, 2008.
- [25] J. Snoek, H. Larochelle, and R. P. Adams, “Practical bayesian optimization of machine learning algorithms,” in *Advances in neural information processing systems*, pp. 2951–2959, 2012.
- [26] P. I. Frazier, “A tutorial on bayesian optimization,” *arXiv preprint arXiv:1807.02811*, 2018.
- [27] A. Klein, S. Falkner, S. Bartels, P. Hennig, and F. Hutter, “Fast bayesian optimization of machine learning hyperparameters on large datasets,” in *Artificial Intelligence and Statistics*, pp. 528–536, PMLR, 2017.
- [28] J. T. Springenberg, A. Klein, S. Falkner, and F. Hutter, “Bayesian optimization with robust bayesian neural networks,” in *Proceedings of the 30th International Conference on Neural Information Processing Systems*, pp. 4141–4149, 2016.
- [29] J. Mockus, *Bayesian approach to global optimization: theory and applications*, vol. 37. Springer Science & Business Media, 2012.
- [30] R. Hassan, B. Cohanin, O. De Weck, and G. Venter, “A comparison of particle swarm optimization and the genetic algorithm,” in *46th AIAA/ASME/ASCE/AHS/ASC structures, structural dynamics and materials conference*, p. 1897, 2005.
- [31] A. H. Wright, “Genetic algorithms for real parameter optimization,” in *Foundations of genetic algorithms*, vol. 1, pp. 205–218, Elsevier, 1991.
- [32] D. P. Bertsekas, D. P. Bertsekas, D. P. Bertsekas, and D. P. Bertsekas, *Dynamic programming and optimal control*, vol. 1. Athena scientific Belmont, MA, 1995.
- [33] K. Zhou, J. C. Doyle, K. Glover, *et al.*, *Robust and optimal control*, vol. 40. Prentice hall New Jersey, 1996.

- [34] R. S. Sutton and A. G. Barto, *Reinforcement learning: An introduction*. MIT press, 2018.
- [35] L. P. Kaelbling, M. L. Littman, and A. W. Moore, “Reinforcement learning: A survey,” *Journal of artificial intelligence research*, vol. 4, pp. 237–285, 1996.
- [36] A. Gelman, J. B. Carlin, H. S. Stern, D. B. Dunson, A. Vehtari, and D. B. Rubin, *Bayesian data analysis*. CRC press, 2013.
- [37] P. J. Green, “Reversible jump markov chain monte carlo computation and bayesian model determination,” *Biometrika*, vol. 82, no. 4, pp. 711–732, 1995.
- [38] D. Gamerman and H. F. Lopes, *Markov chain Monte Carlo: stochastic simulation for Bayesian inference*. CRC Press, 2006.
- [39] C. K. Williams and C. E. Rasmussen, “Gaussian processes for regression,” in *Advances in neural information processing systems*, pp. 514–520, 1996.
- [40] C. K. Williams and C. E. Rasmussen, *Gaussian processes for machine learning*, vol. 2. MIT press Cambridge, MA, 2006.
- [41] P. I. Frazier, W. B. Powell, and S. Dayanik, “A knowledge-gradient policy for sequential information collection,” *SIAM Journal on Control and Optimization*, vol. 47, no. 5, pp. 2410–2439, 2008.
- [42] P. Frazier, W. Powell, and S. Dayanik, “The knowledge-gradient policy for correlated normal beliefs,” *INFORMS journal on Computing*, vol. 21, no. 4, pp. 599–613, 2009.
- [43] I. O. Ryzhov, “On the convergence rates of expected improvement methods,” *Operations Research*, vol. 64, no. 6, pp. 1515–1528, 2016.
- [44] S. E. Chick, J. Branke, and C. Schmidt, “Sequential sampling to myopically maximize the expected value of information,” *INFORMS Journal on Computing*, vol. 22, no. 1, pp. 71–80, 2010.
- [45] K. Chaloner and I. Verdinelli, “Bayesian experimental design: A review,” *Statistical Science*, pp. 273–304, 1995.
- [46] J. Wu, S. Toscano-Palmerin, P. I. Frazier, and A. G. Wilson, “Practical multi-fidelity bayesian optimization for hyperparameter tuning,” in *Uncertainty in Artificial Intelligence*, pp. 788–798, PMLR, 2020.
- [47] S. Chen, K.-R. G. Reyes, M. K. Gupta, M. C. McAlpine, and W. B. Powell, “Optimal learning in experimental design using the knowledge gradient policy with application to characterizing nanoemulsion stability,” *SIAM/ASA Journal on Uncertainty Quantification*, vol. 3, no. 1, pp. 320–345, 2015.
- [48] J. M. Bernardo and R. Rueda, “Bayesian hypothesis testing: A reference approach,” *International Statistical Review*, vol. 70, no. 3, pp. 351–372, 2002.
- [49] F. D. Schönbrodt, E.-J. Wagenmakers, M. Zehetleitner, and M. Perugini, “Sequential hypothesis testing with bayes factors: Efficiently testing mean differences,” *Psychological methods*, vol. 22, no. 2, p. 322, 2017.

- [50] J. A. Hoeting, D. Madigan, A. E. Raftery, and C. T. Volinsky, “Bayesian model averaging: a tutorial,” *Statistical science*, pp. 382–401, 1999.
- [51] X. He, K. G. Reyes, and W. B. Powell, “Optimal learning with local nonlinear parametric models over continuous designs,” *SIAM Journal on Scientific Computing*, vol. 42, no. 4, pp. A2134–A2157, 2020.
- [52] K. Monteith, J. L. Carroll, K. Seppi, and T. Martinez, “Turning bayesian model averaging into bayesian model combination,” in *The 2011 International Joint Conference on Neural Networks*, pp. 2657–2663, IEEE, 2011.
- [53] Y. Wang, K. G. Reyes, K. A. Brown, C. A. Mirkin, and W. B. Powell, “Nested-batch-mode learning and stochastic optimization with an application to sequential multistage testing in materials science,” *SIAM Journal on Scientific Computing*, vol. 37, no. 3, pp. B361–B381, 2015.
- [54] K. Reyes, S. Chen, Y. Li, and W. B. Powell, “Quantifying experimental characterization choices in optimal learning and materials design,” in *TMS 2015 144th Annual Meeting & Exhibition*, pp. 697–704, Springer, Cham, 2015.
- [55] W. B. Powell, *Approximate Dynamic Programming: Solving the curses of dimensionality*, vol. 703. John Wiley & Sons, 2007.
- [56] C. J. Watkins and P. Dayan, “Q-learning,” *Machine learning*, vol. 8, no. 3-4, pp. 279–292, 1992.
- [57] C. B. Browne, E. Powley, D. Whitehouse, S. M. Lucas, P. I. Cowling, P. Rohlfshagen, S. Tavener, D. Perez, S. Samothrakis, and S. Colton, “A survey of monte carlo tree search methods,” *IEEE Transactions on Computational Intelligence and AI in games*, vol. 4, no. 1, pp. 1–43, 2012.
- [58] R. Coulom, “Efficient selectivity and backup operators in monte-carlo tree search,” in *International conference on computers and games*, pp. 72–83, Springer, 2006.
- [59] B. R. Group *et al.*, “The relativistic heavy ion collider project at brookhaven,” *Nuclear Physics A*, vol. 478, pp. 861–873, 1988.
- [60] X. Luo and N. Xu, “Search for the qcd critical point with fluctuations of conserved quantities in relativistic heavy-ion collisions at rhic: an overview,” *Nuclear Science and Techniques*, vol. 28, no. 8, p. 112, 2017.
- [61] A. Bazavov, H.-T. Ding, P. Hegde, O. Kaczmarek, F. Karsch, E. Laermann, S. Mukherjee, H. Ohno, P. Petreczky, E. Rinaldi, H. Sandmeyer, C. Schmidt, C. Schroeder, S. Sharma, W. Soeldner, R. A. Soltz, P. Steinbrecher, and P. M. Vranas, “Skewness and kurtosis of net baryon-number distributions at small values of the baryon chemical potential,” *Phys. Rev. D*, vol. 96, p. 074510, Oct 2017.
- [62] M. Aggarwal, Z. Ahammed, A. Alakhverdyants, I. Alekseev, J. Alford, B. Anderson, D. Arkhipkin, G. Averichev, J. Balewski, L. Barnby, *et al.*, “Higher moments of net proton multiplicity distributions at rhic,” *Physical review letters*, vol. 105, no. 2, p. 022302, 2010.
- [63] J. Thäder, S. collaboration, *et al.*, “Higher moments of net-particle multiplicity distributions,” *Nuclear Physics A*, vol. 956, pp. 320–323, 2016.